SERTS-95 MEASUREMENTS OF WAVELENGTH SHIFTS IN CORONAL EMISSION LINES ACROSS A SOLAR ACTIVE REGION

JEFFREY W. BROSIUS,[1] ROGER J. THOMAS, AND JOSEPH M. DAVILA
Code 682, NASA/Goddard Space Flight Center, Greenbelt, MD 20771

ABSTRACT

We used slit spectra from the 1995 flight of Goddard Space Flight Center's Solar EUV Rocket Telescope and Spectrograph (SERTS-95) to measure wavelength shifts of coronal emission lines in the core of NOAA active region 7870 relative to its immediate surroundings (its "edge"). This method circumvents the unavailability of reliable laboratory rest wavelengths for the observed lines by using wavelengths from the edge spectrum as references. We derived the SERTS-95 wavelength calibration from measurements of a post-flight laboratory spectrum containing 28 He II and Ne II EUV standard wavelengths known to high accuracy. Wavelength measurements for lines of He I, Ne III, and additional lines of Ne II in the laboratory calibration spectrum provide more accurate values than were previously available, enabling these lines also to serve as future calibration standards. Six solar lines were chosen for this study, namely, He II at 303.78 Å, Fe XII at 193.51 Å, Fe XIII at 202.05 Å, Fe XIV at 211.33 Å, Fe XV at 284.15 Å, and Fe XVI at 335.41 Å. Because these lines are free from known blends in the SERTS-95 spectra and are either intrinsically strong or near the SERTS-95 peak sensitivity, they are our most reliable lines for measuring relative wavelength shifts in the spatially resolved active-region core spectra. The iron ions are the hottest ions ever used for this type of analysis. All six lines reveal statistically significant spatial variations in their measured relative wavelength shifts in the active-region core, including mixtures of blueshifts and redshifts (each with maximum values corresponding to relative Doppler velocities ~ 15 km s^{-1}), indicating a dynamic, turbulent corona. For each of these lines we calculated weighted-average relative Doppler velocities from the wavelength shifts in the spatially resolved core spectra by weighting the shifts in the individual spatial pixels with their respective measurement uncertainties. This yields velocities of 3.3 ± 1.1 km s^{-1} for He II, 5.2 ± 1.6 km s^{-1} for Fe XII, 0.7 ± 1.5 km s^{-1} for Fe XIII, -2.1 ± 1.4 km s^{-1} for Fe XIV, 1.0 ± 1.1 km s^{-1} for Fe XV, and -1.1 ± 0.8 km s^{-1} for Fe XVI. We also calculated intensity-weighted relative Doppler velocities from the wavelength shifts in the spatially averaged core spectrum, obtaining corresponding values of 5.8 ± 0.6 km s^{-1}, 5.7 ± 0.9 km s^{-1}, 0.4 ± 0.7 km s^{-1}, -2.1 ± 1.0 km s^{-1}, 0.8 ± 0.8 km s^{-1}, and -1.1 ± 0.5 km s^{-1}. Combining the above six lines with several additional ones that are strong enough in both the edge and average core spectra to provide reliable centroid measurements, we find statistically significant net relative redshifts for lines of He II, Fe X, Fe XI, and Fe XII; lines of Fe XIII and Fe XV show no significant shift while lines of Si XI, Fe XIV, and Fe XVI show a small net relative blueshift. Where multiple lines are available for a given ion, the directions (red or blue) and magnitudes (except for Fe XI) of the relative shifts are mutually consistent. The net relative blueshift observed in the hottest active-region coronal lines in our sample, combined with the net relative redshift observed in the cooler active-region coronal lines, suggests a net upflow of heated material cospatially and cotemporally with a net downflow of cooler material.

Subject headings: instrumentation: spectrographs — Sun: activity — Sun: corona — Sun: UV radiation

1. INTRODUCTION

Redshifts have been observed in spectral lines emitted from the lower solar transition region for more than two decades. Doschek, Feldman, & Bohlin (1976) used ultraviolet spectra obtained with the normal-incidence slit-spectrograph on *Skylab* to measure redshifts (relative to chromospheric reference lines) of Si IV, C IV, O IV, and N V lines observed in quiet-Sun and coronal hole areas, the largest shift implying a downflow velocity ~ 15 km s^{-1}. Rest wavelengths were measured in solar limb spectra and found to agree with wavelengths tabulated by Kelly & Palumbo (1973). No significant shift was observed in O V, the hottest ion in their sample. Feldman, Cohen, & Doschek (1982) extended this work to include active regions, measuring redshifts corresponding to downflow

velocities between 4 and 17 km s^{-1} with the largest shifts occurring for lines formed between about 5×10^4 and 10^5 K. The O V emission from active regions showed significantly smaller redshifts than emission from the other ions.

Subsequent observations have both confirmed the net redshift of the lower transition region lines and extended measurements of the phenomenon to higher temperatures (Dere 1982; Dere, Bartoe, & Brueckner 1984; Hassler, Rottman, & Orrall 1991; Brekke 1993; Brekke, Hassler, & Wilhelm 1997a). Dere (1982) used active-region plage and sunspot observations obtained with the NRL High Resolution Telescope and Spectrograph (HRTS) sounding rocket experiment to measure typical downflow velocities ~ 10 km s^{-1} at log $T \sim 5.0$, with lower velocities at lower and higher temperatures. He extended the observed redshift phenomenon to O V (formed at log $T \sim 5.37$) and Fe XII (log $T \sim 6.14$), although the Fe XII lines are weak and their corresponding measurement uncertainties so large that

[1] Raytheon ITSS, 4400 Forbes Boulevard, Lanham, MD 20706

their redshifts are not statistically significant. Dere, Bartoe, & Brueckner (1984) found an average redshift corresponding to 5 km s^{-1} in the quiet Sun using the two strong C IV resonance lines at 1548.2 and 1550.7 Å (formed at log $T = 5.0$), while Brekke (1993) used HRTS spectra to measure average redshifts in O V lines that can be interpreted as downflow velocities ~ 8 km s^{-1} in the quiet Sun.

Hassler, Rottman, & Orrall (1991) conducted an in-flight wavelength calibration of the LASP EUV Coronal Spectrometer during a 1987 sounding rocket experiment, allowing them to directly measure wavelengths of observed solar lines against platinum lines of known wavelength generated onboard. Solar wavelengths measured above the limb agreed with laboratory values. The C IV line at 1548 Å and Fe II line at 1563 Å yielded net redshifts corresponding to Doppler velocities of 7.5 ± 1.0 km s^{-1} and 2.7 ± 1.5 km s^{-1}, respectively, in the quiet Sun. The Si II line at 1533 Å and Ne VIII line at 770 Å yielded no net redshifts. Brekke et al. (1997a) used the SUMER (Solar Ultraviolet Measurements of Emitted Radiation) spectrometer aboard the *SOHO* (*Solar and Heliospheric Observatory*) spacecraft to find systematic redshifts in transition region as well as coronal lines, extending the temperature range of the phenomenon to O VI (log $T \sim 5.46$), Ne VIII (log $T \sim 5.80$), and Mg X (log T ~ 6.05). These results must be viewed with some caution since, as the authors point out, conflicting reference wavelengths have been reported for O VI and Mg X. Further, the Mg X reference wavelength that they adopted (624.95 Å, from Kelly 1987) is given to only two decimal places (not three or four), indicating the relative uncertainty in its value.

Hassler, Rottman, & Orrall (1991) found that the solar rest wavelengths determined by comparison with their onboard Pt lamp all agreed with laboratory values within the measurement uncertainty, and Feldman, Cohen, & Doschek (1982) detected no redshifts above the limb. However, Dere, Bartoe, & Brueckner (1984) reported a net redshift at and above the limb, while Brekke (1993) pointed out that high-resolution HRTS observations suggest the presence of local small-scale horizontal flow fields above the limb that can introduce systematic error when using the off-limb position as a reference. Brekke, Kjeldseth-Moe, & Harrison (1997c) used the CDS/NIS (Coronal Diagnostic Spectrometer's Normal Incidence Spectrometer) on *SOHO* to measure O V 629 Å profiles at various positions along an active-region loop above the limb. Relative to the average profile of the same line from an extended quiet area at Sun center (which itself may be shifted relative to the chromosphere or to an absolute reference system), the authors measured blueshifts in excess of 60 km s^{-1} and redshifts in excess of 50 km s^{-1}, with an estimated accuracy ~ 10 km s^{-1}. This hints at potential hazards when using even off-limb spectra to measure solar "rest wavelengths."

In the present work we use 170–340 Å spatially resolved ($\sim 5'' \times 4''.4$ pixels) EUV spectra of a solar active region and its environs obtained during the 1995 sounding rocket flight of Goddard Space Flight Center's Solar EUV Rocket Telescope and Spectrograph (SERTS-95) to seek wavelength shifts of coronal emission lines from various ion species, including He II, Si XI, and Fe X–XVI. Unfortunately, the absolute rest wavelengths for most lines in this wave-band are not well known. For example, the Kelly (1987) finding list and the Fuhr, Martin, & Wiese (1988) atomic parameter compilation both adopt wavelengths for almost all of their Fe XI–XV lines in this wave band from the solar observations

of Behring et al. (1976) or Behring, Cohen, & Feldman (1972). Thus the "standard" wavelengths for the lines used in the present work are already referenced to their apparent solar values.

Behring et al. (1976) obtained a full-Sun solar spectrum from 160 to 770 Å on photographic plates during a sounding rocket flight in 1973. Their wavelength scale is based entirely on the wavelengths of 10 strong lines of He I, He II, O III, O IV, O V, and Ne VII compiled in Kelly & Palumbo (1973). However, the O IV and O V ions used by Behring et al. (1976) to derive their wavelength calibration were later found to exhibit persistent redshifts in a variety of solar features (Doschek et al. 1976; Feldman et al. 1982; Dere 1982; Brekke 1993; Brekke et al. 1997a). Further, Brekke et al. (1997a) also found redshifts in lines of Ne VIII, formed at a similar temperature (log $T \sim 5.80$) to the Ne VII line (log $T \sim 5.71$) used as a wavelength standard by Behring et al. (1976). The Behring et al. (1972) wavelength scale was also derived from standard laboratory wavelengths, but the standards used are not listed in their paper. Nevertheless, the wavelengths compiled by Kelly (1987) for lines of Fe XI, XII, XIII, XIV, and XV, many of which are adopted from the two Behring references, are not laboratory rest values, but are likely affected by whatever mechanism produces the observed solar wavelength shifts. It would, therefore, be meaningless to compare our derived SERTS-95 wavelengths with those from Kelly (1987) in search of net wavelength shifts. This underscores a need for improved laboratory and/or theoretical values for wavelengths from these coronal iron ions.

To circumvent the absence of true laboratory rest wavelengths for the coronal iron ions in the SERTS-95 spectrum, we restrict our analysis here to a search for wavelength shifts in the active-region "core" relative to the area directly adjacent to the region, i.e., its "edge". Section 2 describes the SERTS-95 wavelength calibration, § 3 presents the solar observations, § 4 provides wavelength shift measurements, § 5 discusses implications of the measured shifts, and § 6 summarizes our conclusions.

2. WAVELENGTH CALIBRATION

The SERTS-95 wavelength calibration was derived from laboratory EUV spectra of a hollow-cathode gas-discharge lamp recorded on photographic film and digitized shortly after the flight. Laboratory spectra were averaged over the length of the slit to reduce the noise. The background for the average spectrum was calculated by removing emission lines, replacing them with appropriate local averages, and smoothing the remainder. This background was then subtracted from the initial averaged spectrum, leaving only an average laboratory emission line spectrum (with noise) on a zero base-level. The centroid pixel positions of 2 He I lines, 3 He II lines, 31 Ne II lines, and 14 Ne III lines were derived from Gaussian fits to line profiles in the average, background-corrected spectrum. Of these, the 3 He II lines and 25 of the Ne II lines have rest wavelengths that are known to better than 0.3 mÅ (Kaufman & Edlen 1974). We used these lines, listed in Table 1, to derive the SERTS-95 wavelength scale as follows.

Since the He II line at 303.78 Å is strong in both the laboratory and the solar spectra, we use it as the reference wavelength on which the solar spectrum is fixed to the laboratory wavelength scale. We therefore expressed the measured centroid positions of all the lines detected in

TABLE 1
SERTS-95 WAVELENGTH CALIBRATION FROM A POST-FLIGHT LABORATORY SPECTRUM

Number	Centroid Pixel	Ion	SERTS Wavelength	Standard Wavelength	Residual (mÅ)
1	−5537.0211	He II	243.0265 ± 0.0008	243.0266	−0.1
2	−4325.9009	He II	256.3147 ± 0.0004	256.3170	−2.3
3	0.0000	He II	303.7823 ± 0.0002	303.7822	0.1
4	1894.3554	Ne II	324.5702 ± 0.0014	324.5686	1.6
5	2073.5187	Ne II	326.5363 ± 0.0006	326.5376	−1.3
6	2096.3044	Ne II	326.7864 ± 0.0004	326.7856	0.8
7	2139.3564	Ne II	327.2588 ± 0.0007	327.2605	−1.7
8	2172.3959	Ne II	327.6214 ± 0.0005	327.6210	0.4
9	2461.0754	Ne II	330.7893 ± 0.0011	330.7887	0.6
10	4416.0693	Ne II	352.2428 ± 0.0010	352.2436	−0.8
11	4480.9183	Ne II	352.9544 ± 0.0003	352.9549	−0.5
12	4504.7333	Ne II	353.2157 ± 0.0005	353.2145	1.2
13	4569.8533	Ne II	353.9303 ± 0.0016	353.9297	0.6
14	4663.8173	Ne II	354.9614 ± 0.0007	354.9620	−0.6
15	4727.0773	Ne II	355.6556 ± 0.0013	355.6550	0.6
16	4753.4643	Ne II	355.9452 ± 0.0020	355.9480	−2.8
17	4770.1813	Ne II	356.1286 ± 0.0011	356.1288	−0.2
18	4798.7543	Ne II	356.4422 ± 0.0012	356.4399	2.3
19	4807.5903	Ne II	356.5391 ± 0.0028	356.5398	−0.7
20	4831.3693	Ne II	356.8001 ± 0.0009	356.8001	0.0
21	4898.3633	Ne II	357.5352 ± 0.0003	357.5346	0.6
22	5253.3963	Ne II	361.4312 ± 0.0003	361.4321	−0.9
23	5346.6673	Ne II	362.4547 ± 0.0003	362.4544	0.3
24	9301.8243	Ne II	405.8541 ± 0.0004	405.8538	0.3
25	9418.8283	Ne II	407.1379 ± 0.0002	407.1377	0.2
26	12873.612	Ne II	445.0405 ± 0.0004	445.0393	1.2
27	12984.326	Ne II	446.2551 ± 0.0003	446.2552	−0.1
28	13014.765	Ne II	446.5890 ± 0.0004	446.5902	−1.2

NOTE—The centroid pixel is the distance of the various line centroids from that of the He II line at 303.782 Å in units of 5 μm pixels. The SERTS and standard wavelengths are in Å, and the residuals are in mÅ. Tabulated uncertainties on the measured wavelengths are statistical only; an additional systematic uncertainty of 0.0011 Å is also present, as described in the text.

the laboratory spectrum relative to the He II line at 303.78 Å (see Table 1). The wavelength scale was obtained by fitting a third-order polynomial to the 28 standard wavelengths (λ in Å) known to high accuracy as a function of centroid pixel distance (d, in pixel numbers) from the He II 303.78 Å centroid. The resulting polynomial is

$$N\lambda = 303.78230 + (0.010973498)d$$
$$+ (8.8947177 \times 10^{-11})d^2$$
$$- (1.1745010 \times 10^{-14})d^3 , \qquad (1)$$

where N is the spectral order (1 or 2). Table 1 gives the fitted values of the 28 standard wavelengths along with their corresponding statistical uncertainties. Differences between the fitted wavelengths and the standard wavelengths are listed as "residuals" and expressed in mÅ. The overall goodness of the fit is quantified by its small standard deviation, 1.1 mÅ. This value should be incorporated into the statistical uncertainties on each of the laboratory wavelengths listed in Table 1 to get the total uncertainty, $\sigma_{total} = (0.0011^2 + \sigma_{statistical}^2)^{1/2}$ Å.

In addition to the 28 standards of Table 1 used to derive the instrument's wavelength scale, the SERTS post-flight laboratory spectra also include two He I lines, 6 Ne II lines, 14 Ne III lines, and one unidentified line, most of whose wavelengths had previously been known to an accuracy of no better than 10 mÅ (Kelly 1987). Inserting their measured centroid pixel positions into equation (1), we can establish

much more accurate wavelengths for these lines, as listed in Table 2, even with the added systematic uncertainty described above (which has been included in Table 2). Thus the 23 new lines in Table 2 may serve as additional EUV wavelength standards for future studies, though with somewhat lower accuracy than the primary standards.

The systematic uncertainties in the SERTS-95 wavelength scale are important when deriving absolute wavelengths of either laboratory or solar emission lines; however, since in what follows we deal only with *differences* between wavelengths measured with a common wavelength scale in two different solar features, the systematic uncertainties cancel out.

3. OBSERVATIONS

SERTS was launched on a Terrier-boosted Black Brant rocket from White Sands, NM, at 1800 UT on 1995 May 15. It reached a maximum altitude of 307 km and recorded spectrographic data on photographic film for nearly 7 minutes. This was the last flight for which data were recorded on film: subsequent flights have used a CCD-intensified detector. SERTS-95 included a multilayer-coated toroidal diffraction grating that enhanced the instrumental sensitivity over that of a standard gold-coated grating in the second-order wave band (∼171–223 Å). First-order lines between ∼240 and 340 Å were also observed. The instrument performed well, obtaining four exposures in each of two different pointing positions.

TABLE 2

New EUV Standard Wavelengths of He I, Ne II, and Ne III Lines from the SERTS Post-Flight Wavelength Calibration

Number	Ion	Previous Wavelength	SERTS Wavelength
1........	Ne III	267.07	267.0256 ± 0.0018
2........	Ne III	267.53	267.4884 ± 0.0019
3........	Ne III	267.71	267.6870 ± 0.0025
4........	Ne III	282.49	282.4948 ± 0.0022
5........	Ne III	283.15, 283.17	283.1745 ± 0.0014
6........	Ne III	283.66	283.6651 ± 0.0015
7........	Ne III	283.87	283.8710 ± 0.0047
8........	Ne III	301.12	301.1242 ± 0.0013
9........	...	...	304.8793 ± 0.0017
10	He I	305.4	305.6112 ± 0.0020
11	Ne III	308.56	308.5720 ± 0.0014
12	Ne III	313.05	313.0574 ± 0.0014
13	Ne III	313.68	313.6919 ± 0.0019
14	Ne III	313.92	313.9635 ± 0.0039
15	He I	314.6	314.4507 ± 0.0040
16	Ne II	325.393	325.3916 ± 0.0017
17	Ne II	327.355	327.3474 ± 0.0016
18	Ne II	328.090	328.0880 ± 0.0020
19	Ne II	330.205	330.2129 ± 0.0026
20	Ne II	330.626	330.6389 ± 0.0018
21	Ne II	355.4541	355.4499 ± 0.0016
22	Ne III	379.31	379.3059 ± 0.0013
23	Ne III	427.84	427.8521 ± 0.0018

NOTE.—The SERTS and previous wavelengths are in Å. Because the previous wavelengths listed here are not included in Kaufman & Edlen 1974, we adopt the values compiled by Kelly 1987. Uncertainties on the measured wavelengths include both statistical and systematic contributions.

Spectroheliograms of NOAA active region 7870 (N09 W22) and slit spectra of quiet areas northeast of region 7870 were obtained in the first pointing position; slit spectra of region 7870 and spectroheliograms of quiet areas to the northeast were obtained in the second. The slit spectra used in the present work were obtained from the longest exposure (202.4 s) in the second position. Brosius, Davila, & Thomas (1998) discuss SERTS data analysis techniques, derive the SERTS-95 absolute radiometric calibration, and provide lists of emission lines observed in average active region and quiet spectra.

The absolute pointing of the SERTS-95 observations was derived by co-aligning the He II 303.78 Å spectroheliograms with coordinated, full-disk He I 10830 Å images from the National Solar Observatory/Kitt Peak National Observatory (NSO/KPNO) spectromagnetograph. We found that the center of the SERTS entrance aperture assembly projects onto a point located $213'' \pm 7''$ west and $483'' \pm 7''$ north of solar disk center (in the quiet Sun) for the first pointing position, and $335'' \pm 7''$ west and $198'' \pm 7''$ north (in region 7870) for the second. The narrow slit bisected NOAA region 7870 at a $24°3 \pm 0°2$ angle counterclockwise from the solar rotation axis. Figure 1 shows the SERTS slit projected onto a photospheric longitudinal magnetogram of region 7870 obtained with the NSO/KPNO spectromagnetograph, along with intensity contours of the Fe XVI line at 335.41 Å from the co-aligned SERTS spectroheliogram. The active-region "core" measurements were made from the 88″4 long section of the slit between the two short perpendicular fiducials on the figure. The "edge" measure-

TABLE 3

Spectral Line Data for the Active-Region "Edge" Spectrum

Ion	log T_{max}	Wavelength	Intensity	Width
He II	4.67	303.7823 ± 0.0004	1.64E + 04 ± 1.84E + 03	95.2 ± 4.9
Fe X	5.98	174.5316 ± 0.0013	4.13E + 02 ± 6.35E + 01	37.6 ± 3.5
Fe X	5.98	177.2423 ± 0.0015	2.04E + 02 ± 3.83E + 01	30.7 ± 3.8
Fe XI	6.06	188.2200 ± 0.0008	2.63E + 02 ± 3.25E + 01	47.0 ± 3.0
Fe XI	6.06	192.8190 ± 0.0011	4.36E + 01 ± 6.08E + 00	41.0 ± 3.3
Fe XII	6.14	192.3966 ± 0.0011	1.16E + 02 ± 1.49E + 01	53.1 ± 3.6
Fe XII	6.14	193.5124 ± 0.0005	2.84E + 02 ± 3.29E + 01	49.1 ± 2.7
Fe XII	6.14	195.1255 ± 0.0006	5.35E + 02 ± 6.35E + 01	49.0 ± 2.9
Fe XIII.....	6.20	201.1296 ± 0.0009	1.96E + 02 ± 2.52E + 01	45.2 ± 3.1
Fe XIII.....	6.20	202.0538 ± 0.0003	8.55E + 02 ± 9.73E + 01	49.0 ± 2.6
Fe XIII.....	6.20	203.8346 ± 0.0013	6.68E + 02 ± 8.50E + 01	67.1 ± 4.6
Si XI	6.20	303.3238 ± 0.0013	1.82E + 03 ± 2.19E + 02	89.5 ± 5.4
Fe XIV.....	6.27	211.3339 ± 0.0006	1.23E + 03 ± 1.44E + 02	52.4 ± 3.0
Fe XV	6.33	284.1528 ± 0.0005	5.43E + 03 ± 6.20E + 02	72.6 ± 3.9
Fe XV	6.33	417.2806 ± 0.0029	...	85.0 ± 8.0
Fe XVI......	6.43	335.4112 ± 0.0003	3.87E + 03 ± 4.36E + 02	82.1 ± 4.2

NOTE.—T_{max} is the temperature that maximizes the fractional ion abundance in the available ionization equilibrium calculations. For iron, log T_{max} is derived from quadratic fits to the ionization equilibrium calculations of Arnaud & Raymond 1992; for other elements, it is derived from fits to similar calculations by Monsignori-Fossi (1992, unpublished). Integrated intensities are in ergs cm^2 s^{-1} sr^{-1}. No intensity is listed for the Fe XV line at 417.28 Å because this line lies outside the wavelength range for which the SERTS-95 radiometric calibration was derived; see Brosius et al. 1998. Widths, given in mÅ, are the FWHM intensity including the instrumental profile as well as both thermal and nonthermal contributions. The strongest Fe XI line, at 180.38 Å, is blended with the strong first-order Fe XVI resonance line at 360.76 Å, and so is not usable here. The uncertainties listed for each wavelength are statistical only; systematic uncertainties such as those described in the text are omitted here because they directly cancel out of the wavelength shift measurements on which this work is based.
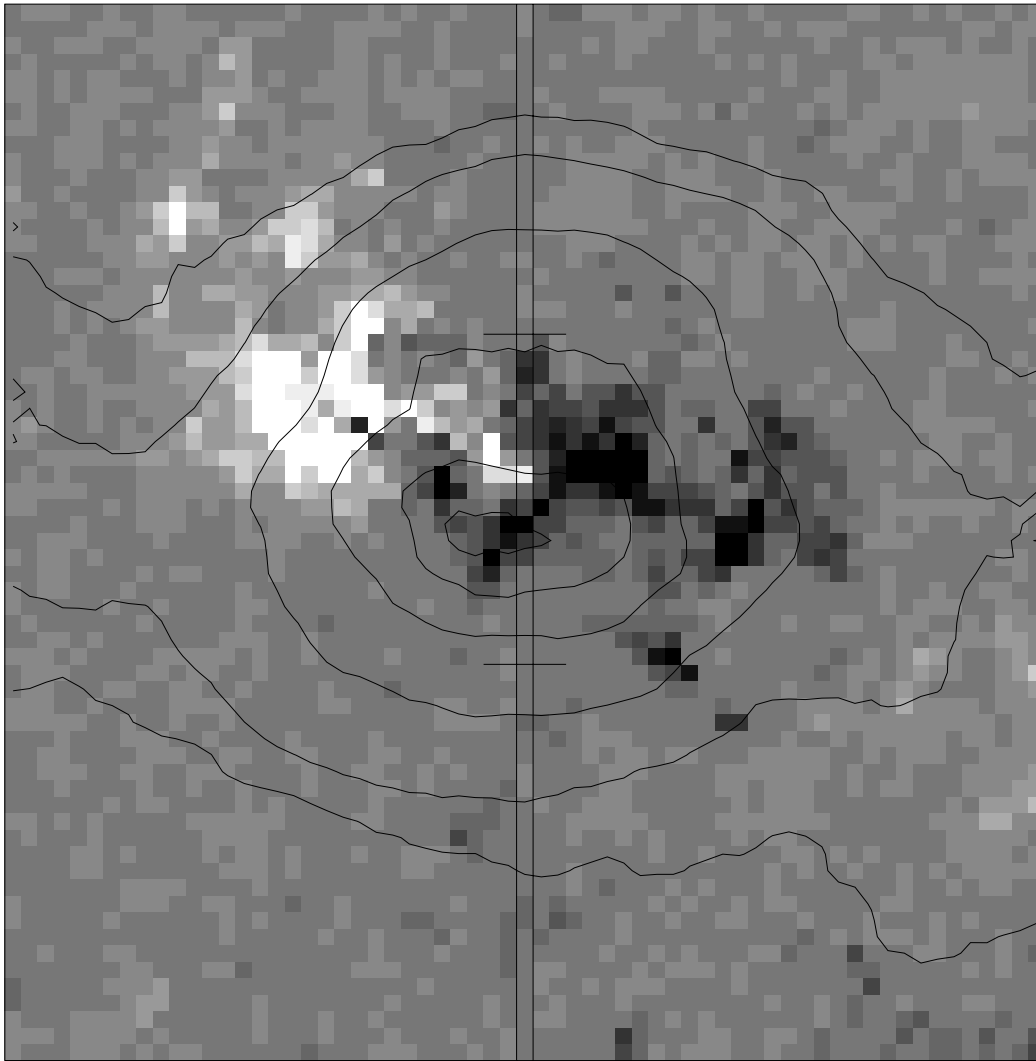
Fig. 1.—Photospheric longitudinal magnetogram of NOAA region 7870 obtained with the NSO/KPNO spectromagnetograph, showing the projection of the SERTS slit along with Fe XVI intensity contours from the co-aligned SERTS spectroheliogram at 335.41 Å. The image dimension is 283″ on each side. Intensity contours are 0.8, 0.6, 0.4, 0.2, 0.1, and 0.07 the maximum image intensity. The boundaries of active-region "edge" and "core" areas are delineated by short lines perpendicular to the slit. The solar rotation axis in this figure is located 24°3 clockwise from the slit.

ments were from sections of the slit above and below these fiducials. The solar rotation axis in this figure is located 24°3 clockwise from the slit.

Spectra were digitized in 64 4″42 spatial pixels along the narrow slit, with each spatial pixel comprised of 20,000 spectral elements. The 20 spatial pixels along the 88″4 segment toward the slit center were designated as active-region "core" because the intensities there are great enough to measure high-quality, low-noise Gaussian profiles in the spatially resolved spectra. Outside the core the line intensities diminish sufficiently that profile fits to all but the very strongest lines yield relatively uncertain values, necessitating spatial averaging in order to reduce the noise. To establish a set of reference wavelengths against which to measure relative shifts in and across the active-region core, we obtained an average "edge" spectrum comprised of the 20 pixels in the 88″4 slit segment northeast of the active region and the 24 pixels in the 106″ slit segment southwest of the region. Wavelengths, intensities, line widths, and their respective uncertainties for the strongest, least noisy lines in the edge spectrum are listed in Table 3. (No intensity is

listed for the Fe XV line at 417.28 Å because this line lies outside the wavelength range for which the SERTS-95 radiometric calibration was derived; see Brosius et al. 1998.) These lines are either intrinsically very strong or else occur in the vicinity of the peak response of the SERTS-95 multilayer-coated toroidal diffraction grating. Additional lines are available but are not used in the present work because the large statistical uncertainties on their fit parameters preclude their utility for reliable wavelength shift measurements. Corresponding values for the average active-region core spectrum are listed in Table 4. Table 4 also expresses the observed wavelength shifts between lines in the core and edge spectra as relative Doppler velocities.

4. RELATIVE WAVELENGTH SHIFTS

The coronal emission lines used in the present analysis to measure relative wavelength shifts (expressed as relative Doppler velocities) between an active-region core and its immediate surroundings come from the hottest ions (Fe XII–XVI, inclusive) ever employed for this purpose. In what follows we measure wavelength shifts of active-region lines

TABLE 4

SPECTRAL LINE DATA FOR THE AVERAGE ACTIVE-REGION CORE SPECTRUM

Ion	Wavelength	Intensity	Width	Profile ΔV	Weighted ΔV
He II	303.7882 ± 0.0005	1.12E + 05 ± 1.27E + 04	85.9 ± 4.4	5.8 ± 0.6	3.3 ± 1.1
Fe X	174.5338 ± 0.0012	1.14E + 03 ± 1.53E + 02	50.5 ± 3.8	3.8 ± 3.0	...
Fe X	177.2477 ± 0.0013	6.24E + 02 ± 8.76E + 01	47.8 ± 3.9	9.1 ± 3.4	...
Fe XI	188.2222 ± 0.0007	6.26E + 02 ± 7.62E + 01	47.7 ± 3.0	3.5 ± 1.7	...
Fe XI	192.8306 ± 0.0016	1.36E + 02 ± 1.99E + 01	53.9 ± 4.8	18.0 ± 3.0	...
Fe XII	192.4007 ± 0.0006	3.37E + 02 ± 3.95E + 01	50.6 ± 2.9	6.4 ± 2.0	...
Fe XII	193.5161 ± 0.0003	7.80E + 02 ± 8.85E + 01	49.6 ± 2.6	5.7 ± 0.9	5.2 ± 1.6
Fe XII	195.1283 ± 0.0005	1.40E + 03 ± 1.62E + 02	51.0 ± 2.8	4.3 ± 1.2	...
Fe XIII.....	201.1299 ± 0.0005	8.88E + 02 ± 1.02E + 02	53.7 ± 2.9	0.4 ± 1.5	...
Fe XIII.....	202.0541 ± 0.0004	1.68E + 03 ± 1.91E + 02	51.5 ± 2.7	0.4 ± 0.7	0.7 ± 1.5
Fe XIII.....	203.8329 ± 0.0011	3.70E + 03 ± 4.47E + 02	71.1 ± 4.3	−2.5 ± 2.5	...
Si XI	303.3216 ± 0.0010	5.76E + 03 ± 6.72E + 02	91.6 ± 5.1	−2.2 ± 1.6	...
Fe XIV.....	211.3324 ± 0.0004	4.28E + 03 ± 4.86E + 02	55.3 ± 2.9	−2.1 ± 1.0	−2.1 ± 1.4
Fe XV	284.1536 ± 0.0005	2.50E + 04 ± 2.86E + 03	65.0 ± 3.5	0.8 ± 0.8	1.0 ± 1.1
Fe XV	417.2791 ± 0.0006	...	97.0 ± 5.1	−1.1 ± 2.1	...
Fe XVI......	335.4100 ± 0.0005	2.28E + 04 ± 2.59E + 03	77.6 ± 4.0	−1.1 ± 0.5	−1.1 ± 0.8

NOTE.—Integrated intensities are in ergs cm^2 s^2 sr^2. No intensity is listed for the Fe XV line at 417.28 Å because this line lies outside the wavelength range for which the SERTS-95 radiometric calibration was derived; see Brosius et al. 1998. Widths, given in mÅ, are the FWHM intensity including the instrumental profile as well as both thermal and nonthermal contributions. The relative Doppler velocities (ΔV) are in km s^{-1}. The uncertainties listed for each wavelength are statistical only; systematic uncertainties such as those described in the text are omitted here because they directly cancel out of the wavelength shift measurements on which this work is based.

relative to their counterparts in the edge spectrum. The success of this effort is made possible by the high spectral resolution (~ 0.06 Å in first order and ~ 0.03 Å in second) of the SERTS instrument. We find a statistically significant net relative redshift between the core and surroundings for lines of He II, Fe X, Fe XI, and Fe XII. We find either no significant shift or a net blueshift for lines of the hotter ions Si XI, Fe XIII, Fe XIV, Fe XV, and Fe XVI. For the six lines appropriate for analysis in spatially resolved spectra, scans across the active-region core reveal relative wavelength shifts ranging from blue (with a minimum value ~ -15 km s^{-1}) to red (with a maximum value $\sim +15$ km s^{-1}) regardless of the net relative shift. For ions from which multiple lines are measurable, the available lines yield mutually consistent shifts: note especially that the three Fe XII lines yield a relative Doppler velocity ~ 5 km s^{-1}, while the three Fe XIII lines and the two Fe XV lines yield values not significantly different from zero.

Because of their relative strength and freedom from known blending, the He II line at 303.78 Å, the Fe XII line at 193.51 Å, the Fe XIII line at 202.05 Å, the Fe XIV line at 211.33 Å, the Fe XV line at 284.15 Å, and the Fe XVI line at 335.41 Å are our best lines for measuring relative wavelength shifts as functions of position in the active-region core. (The Fe XII line at 195.12 Å and the Fe XIII line at 203.83 Å, although quite strong, are known self-blends, so that measurements of wavelength shifts with these lines may be compromised by variations in the constituent line intensities.) Figures 2–7 show profiles of these lines in (panel a) the edge spectrum and (panel b) the average active-region core spectrum. Relative wavelength shifts between lines in the edge and average core spectra are illustrated with normalized profiles in (panel c) and expressed as Doppler velocities ("Profile ΔV") in the fifth column of Table 4. Velocities in this column, derived from relative displacements of line profiles in average spectra, are intensity-weighted average relative velocities because the more intense spatial pixels dominate the average line profiles.

Relative Doppler velocities as a function of pixel position across the active-region core are shown in (panel d), and weighted-average values derived from these are listed in the sixth column of Table 4 ("Weighted ΔV"). Relative velocities derived with this method ascribe greater weights to profile fits with smaller uncertainties in the spatially resolved spectra regardless of their intensities; they are, therefore, more representative of typical coronal velocities. (Note however that since more intense lines tend to carry smaller uncertainties on profile fit parameters than weaker lines, the stronger lines will generally contribute more heavily to the weighted-average relative velocities than the weaker lines.) A comparison of the "profile" and "weighted" ΔV values reveals good agreement; the largest difference occurs for He II, where the "profile" ΔV is intensity-weighted toward a higher value than the "weighted" ΔV because the largest redshifts occur in the core center, where the intensities are greatest. The intensity-weighted relative Doppler velocities from the fifth column in Table 4 are plotted as a function of line formation temperature in Figure 8.

Brekke et al. (1997b) argue that the Fe XVI resonance line at 335.41 Å, originally thought to be ideal for studying coronal mass motions with CDS on SOHO, is contaminated with a Mg VIII line at 335.23 Å and should not be used for coronal dynamical studies. Fortunately this is not a problem for SERTS since these two lines are separated by three times the SERTS instrumental width. An examination of the Fe XVI 335.41 Å profiles of Figure 7a and 7b reveals that the Mg VIII line is so weak that it is not clearly evident in the blue wings of the Fe XVI line in either the edge spectrum or the average active-region core spectrum. Recent theoretical work by Bhatia & Thomas (1998), combined with SERTS line intensity measurements from the previous flights, yield intensity ratios of the Mg VIII line at 335.23 Å to the Fe XVI line at 335.41 Å in both active-region and quiet-Sun areas. This is essentially a measure of the potential contamination of the Fe XVI line by the Mg VIII line in CDS spectra. Adopting the Mg VIII $\lambda335.23/\lambda315.02$ inten-
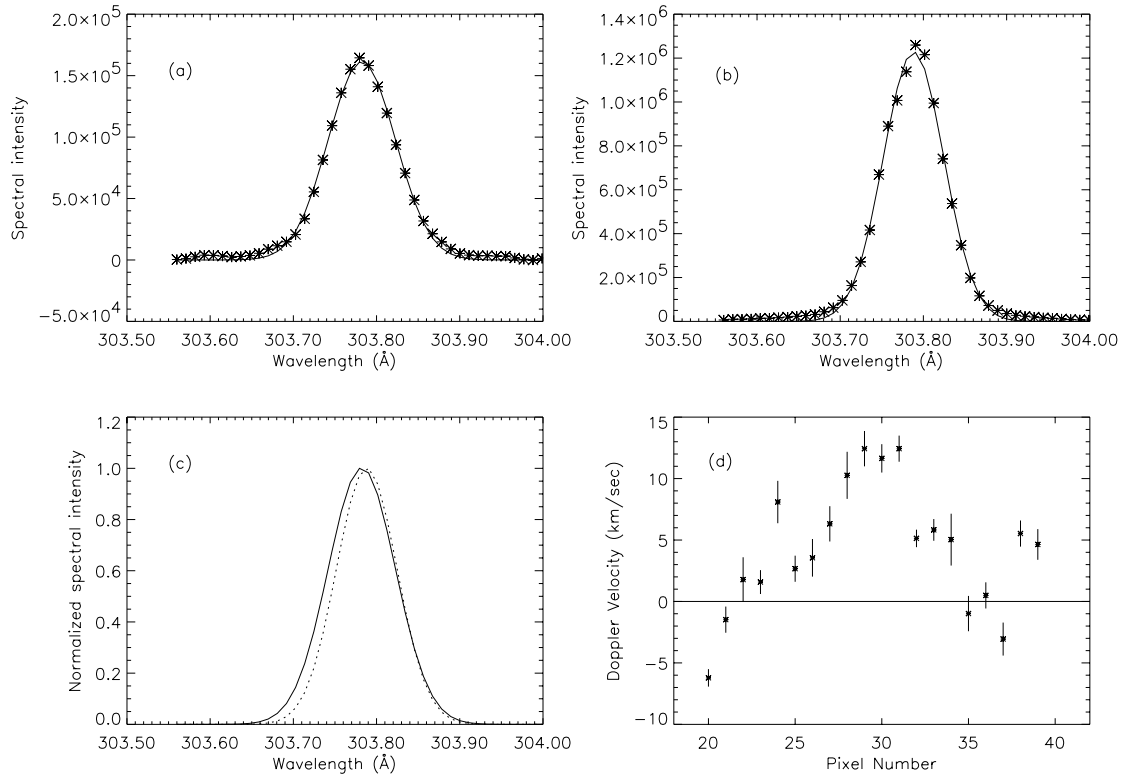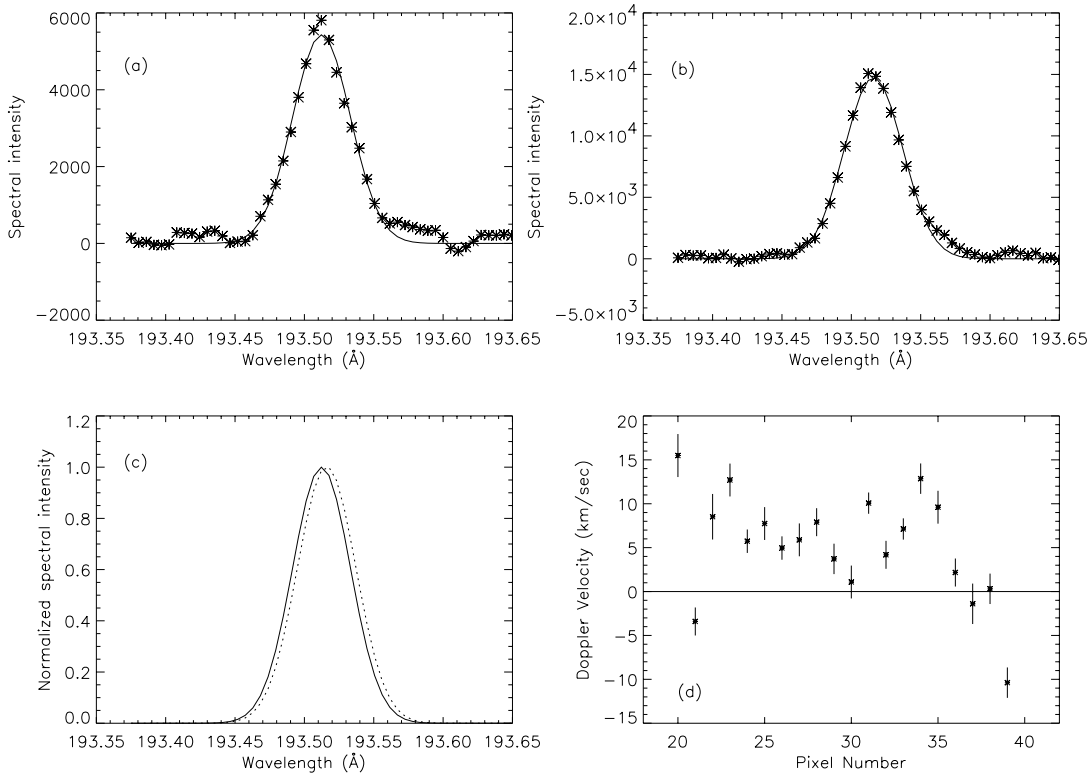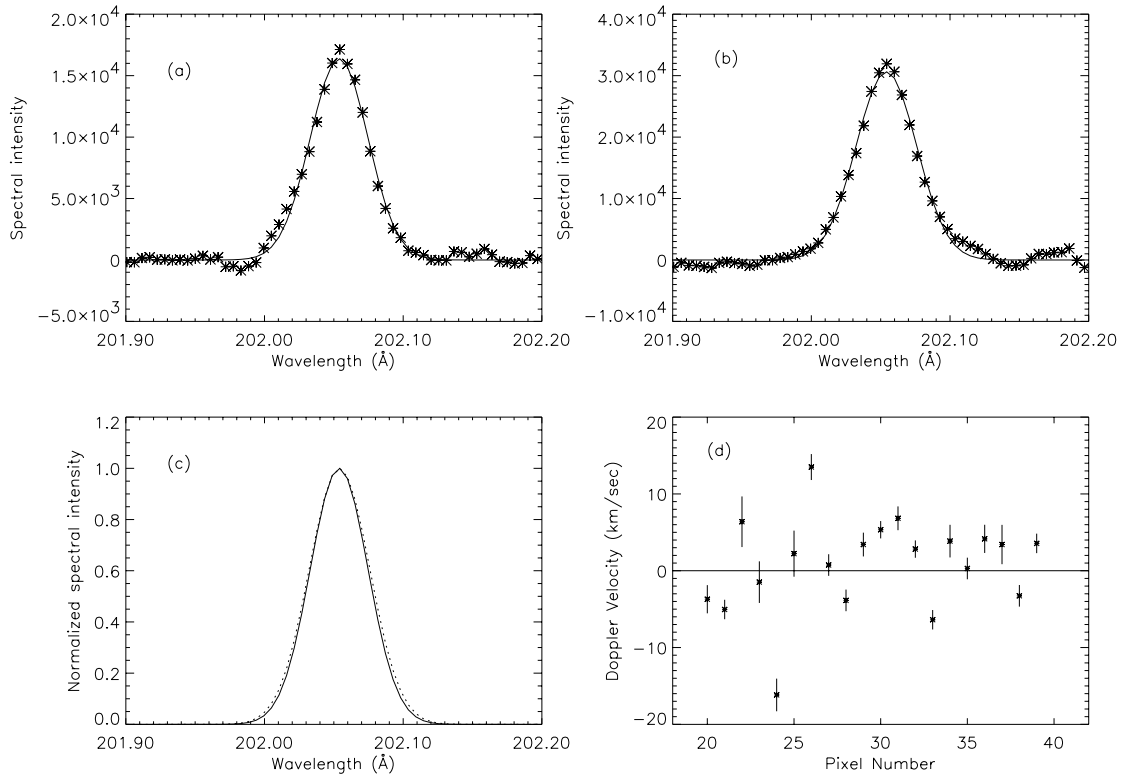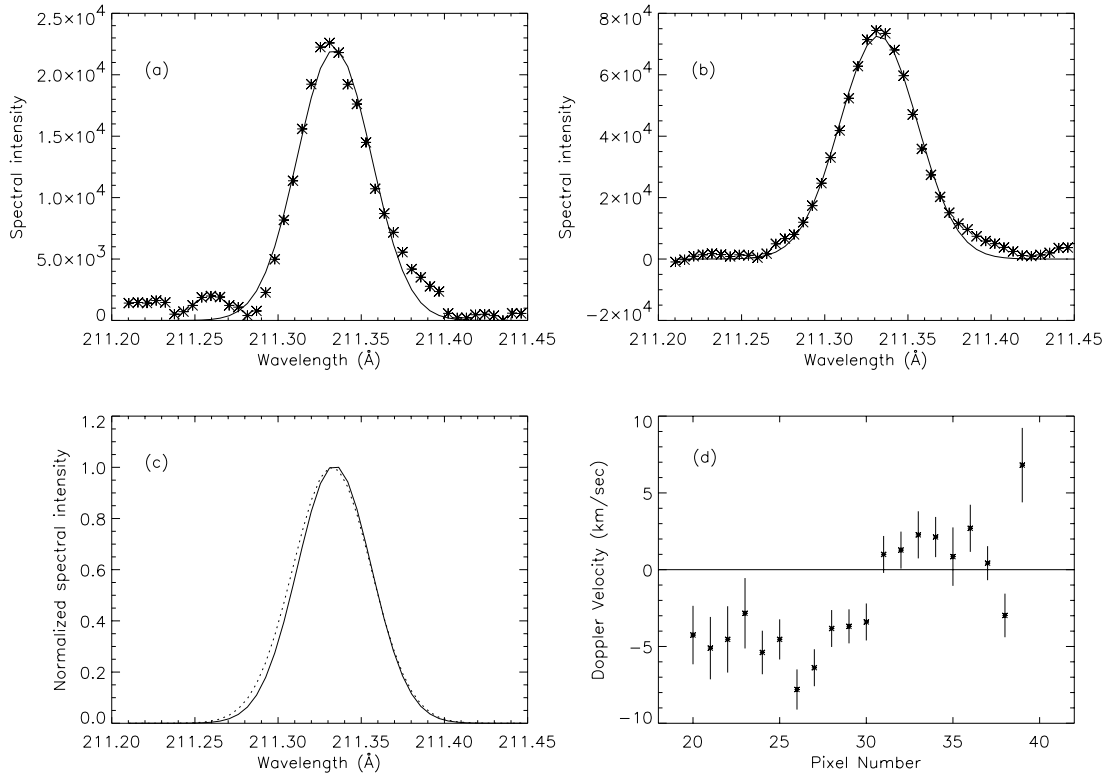
FIG. 2.—He II 303.78 Å (*a*) edge profile; (*b*) average core profile; (*c*) normalized edge (*solid line*) and core (*dotted line*) profiles showing relative centroid shift; (*d*) relative Doppler velocity across active-region core. Spectral intensity is in ergs cm^{-2} s^{-1} sr^{-1} Å^{-1}.

FIG. 3.—Fe XII 193.51 Å (*a*) edge profile; (*b*) average core profile; (*c*) normalized edge (*solid line*) and core (*dotted line*) profiles showing relative centroid shift; (*d*) relative Doppler velocity across active-region core. Spectral intensity is in ergs cm^{-2} s^{-1} sr^{-1} Å^{-1}.
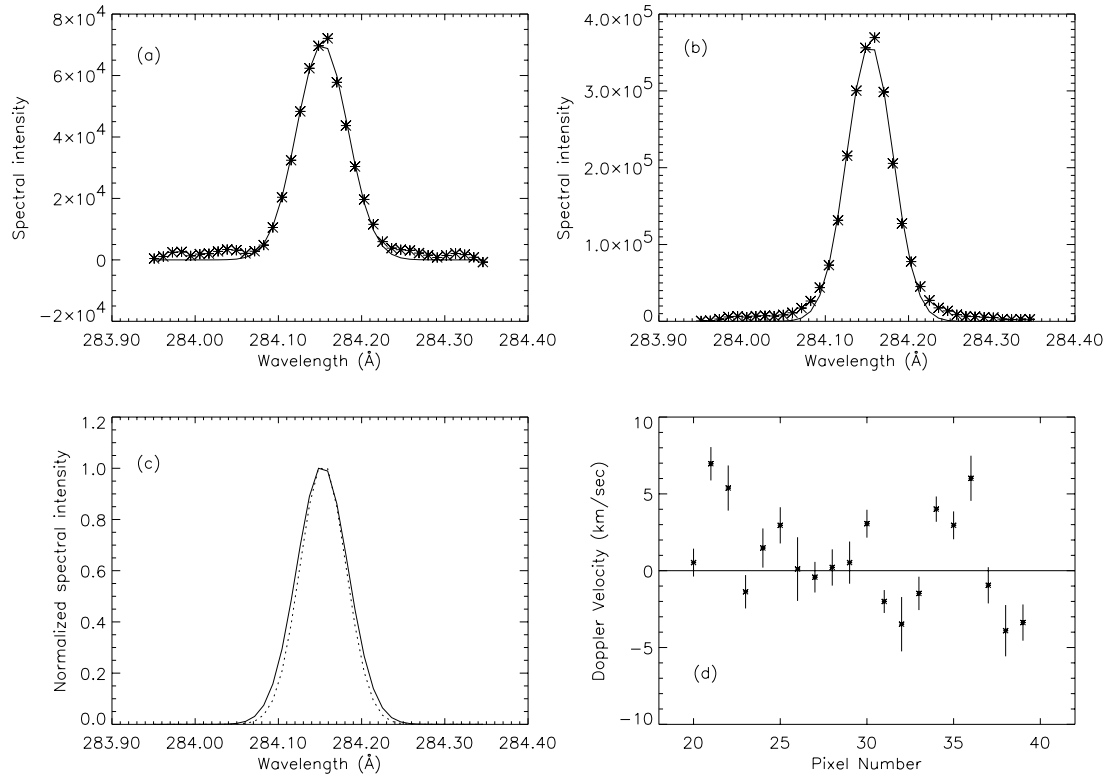
FIG. 4.—Fe XIII 202.05 Å (*a*) edge profile; (*b*) average core profile; (*c*) normalized edge (*solid line*) and core (*dotted line*) profiles showing zero relative shift; (*d*) relative Doppler velocity across active-region core. Spectral intensity is in ergs cm^{-2} s^{-1} sr^{-1} Å^{-1}.

FIG. 5.—Fe XIV 211.33 Å (*a*) edge profile; (*b*) average core profile; (*c*) normalized edge (*solid line*) and core (*dotted line*) profiles showing relative centroid shift; (*d*) relative Doppler velocity across active-region core. Spectral intensity is in ergs cm^{-2} s^{-1} sr^{-1} Å^{-1}.
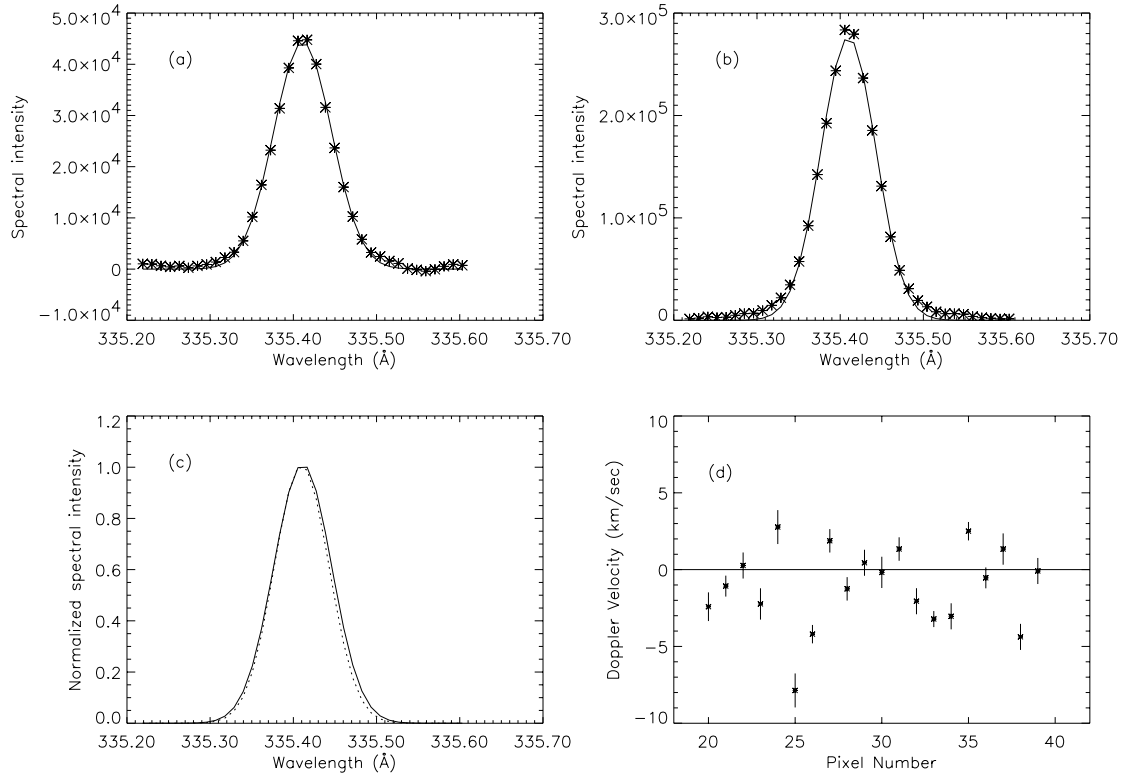
Fig. 6.—Fe xv 284.15 Å (*a*) edge profile; (*b*) average core profile; (*c*) normalized edge (*solid line*) and core (*dotted line*) profiles showing zero relative shift; (*d*) relative Doppler velocity across active-region core. Spectral intensity is in ergs cm^{-2} s^{-1} sr^{-1} Å^{-1}.

Fig. 7.—Fe xvi 335.41 Å (*a*) edge profile; (*b*) average core profile; (*c*) normalized edge (*solid line*) and core (*dotted line*) profiles showing relative centroid shift; (*d*) relative Doppler velocity across active-region core. Spectral intensity is in ergs cm^{-2} s^{-1} sr^{-1} Å^{-1}.
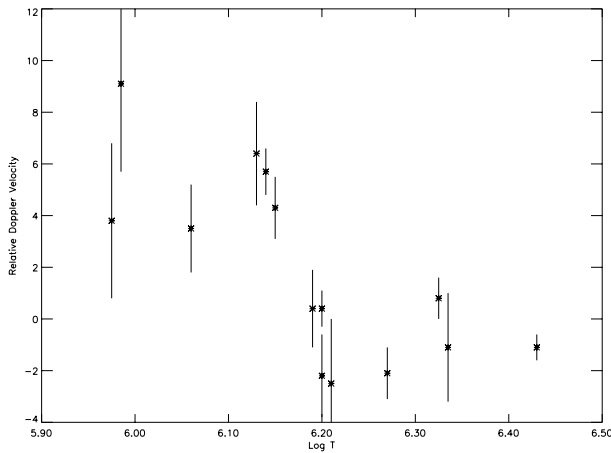
FIG. 8.—Intensity-averaged relative Doppler velocity measurements from the fifth column of Table 4, as a function of line formation temperature. Where multiple lines are measured for a given ion, the data points are displaced from one another to avoid overlap.

sity ratio of 0.205 ± 0.020 (for $8.0 \le \log n_e \le 10.0$) from Bhatia & Thomas (1998) and the SERTS active-region Mg VIII $\lambda 315.02$/Fe XVI $\lambda 335.41$ intensity ratios of 0.0243 for SERTS-89 (Thomas & Neupert 1994), 0.0236 for SERTS-91 and 0.0567 for SERTS-93 (Brosius et al. 1996), and 0.0120 for SERTS-95 (Brosius, Davila, & Thomas 1998), we find Mg VIII $\lambda 335.23$/Fe XVI $\lambda 335.41$ active-region intensity ratios of 0.0050, 0.0048, 0.0116, and 0.0025, respectively. Thus the expected contamination in active-region spectra is very small. Similarly, for the quiet-Sun spectra of SERTS-91 and SERTS-93 (Brosius et al. 1996) we obtain Mg VIII $\lambda 335.23$/Fe XVI $\lambda 335.41$ intensity ratios of 0.074 and 0.055, indicating that blending may indeed become a problem for CDS quiet-Sun spectra.

5. DISCUSSION

Our method of measuring relative wavelength shifts between two different locations on the Sun (i.e., the core and its edge) is necessitated by the unavailability of laboratory rest wavelengths for the EUV coronal lines observed by SERTS. This method has the added advantage of eliminating systematic uncertainties on measured solar wavelengths, as described below. Achour et al. (1995) applied a similar approach to measure transition region differential redshifts between an active region and its quieter surroundings using HRTS spectra. They found a maximum redshift differential of 7 km s^{-1} at 1.35×10^5 K, and no significant shift at 2.3×10^5 K. Although two Fe XII lines were observed in their active-region spectrum, these were not observed in the surroundings, so no redshift differential could be measured at coronal temperatures.

Three sources of systematic uncertainty and one source of statistical uncertainty contribute to the total uncertainty on solar wavelengths derived from SERTS-95. For any given line the statistical uncertainty on its measured wavelength is that derived for the centroid of its Gaussian fit. These values are very small for well-fitted Gaussians such as those shown in Figures 2–7, and are listed in Tables 3 and 4. The first systematic source is that of the actual (solar) wavelength on which the SERTS calibration curve is anchored to the solar spectrum. We assume that the He II line in the edge spectrum is at the laboratory rest wavelength of 303.7823 Å, but

this solar line could in fact be significantly shifted relative to its rest value. Thus all other wavelengths in the SERTS spectrum may be shifted systematically by some unknown amount. The second systematic source is the statistical uncertainty on the centroid position of the He II edge wavelength on which the SERTS calibration curve is anchored to the solar spectrum, meaning that all other wavelengths in the SERTS spectrum may be shifted systematically by this known amount. The third source of systematic uncertainty is that of the wavelength calibration itself, ~ 1.1 mÅ (see § 2). For any given emission line, the sum of these systematic uncertainties on its measured wavelength is the same regardless of spatial position along the SERTS slit. Therefore, these contributions directly cancel out of the net uncertainties on calculated wavelength shifts between two different spatial positions. In other words, each line's measured wavelength is uncertain by an unknown amount whose value remains constant regardless of spatial location; this amount exactly cancels when wavelengths for any given line at two different locations are differenced. The only quantities that contribute to the net measurement uncertainty on wavelength shift between the active-region core (either spatially resolved or spatially averaged) and edge spectra are the statistical uncertainties on the given line in the core and edge spectra.

Dere et al. (1984) found that wavelength shifts of lower transition region lines vary significantly with location on spatial scales of only a few arcseconds. Our finding here of a similar phenomenon for coronal emission lines (witness the statistically significant variation in relative Doppler velocity across the active region as displayed in panel [d] of Figs. 2–7) suggests a common underlying mechanism. No clear pattern for velocity as a function of temperature is evident in the (d) panels of Figures 2–7; indeed, Doppler velocities for lines formed at different temperatures are uncorrelated, the maximum correlation coefficient between any two lines being 0.27. For any given spatial pixel the flow velocity can change sign from one emission line to the next, i.e., no gradual progression from one velocity orientation (red or blue) at a given magnitude to the other orientation with a different magnitude is observed. This indicates that the corona, in addition to being dynamic, is also quite turbulent: adjacent plasma elements, as well as plasma elements along the same line of sight, move independently of one another, at least within the SERTS spatial resolution. Nevertheless, the net blueshift observed in some of the hottest coronal lines coupled with the net redshift observed in the cooler coronal lines (see Fig. 8 and Table 4) suggests a net upflow of heated material cospatially and cotemporally with a net downflow of cooler material.

6. SUMMARY

We derived the SERTS-95 wavelength calibration from measurements of a post-flight laboratory spectrum containing 28 He II and Ne II EUV standard wavelengths known to high accuracy. A third-order polynomial fit yields wavelength as a function of centroid pixel position with a standard deviation of 1.1 mÅ. Wavelength measurements for lines of He I, Ne III, and additional lines of Ne II in the calibration spectrum provide more accurate values than were previously available, enabling these lines also to serve as future calibration standards. We measured wavelength shifts of coronal emission lines in a solar active-region core relative to its immediate surroundings (the edge). This

method removes systematic uncertainties in the SERTS-95 wavelength calibration by cancellation, and circumvents the unavailability of reliable laboratory wavelengths for coronal emission lines by using lines from the edge spectrum as references. Our conclusions are summarized as follows:

1. Because they are free from known blending in the SERTS-95 spectra and are either intrinsically strong or near the peak response of the SERTS-95 multilayer coating, the six lines of He II at 303.78 Å, Fe XII at 193.51 Å, Fe XIII at 202.05 Å, Fe XIV at 211.33 Å, Fe XV at 284.15 Å, and Fe XVI at 335.41 Å are our most reliable lines for measuring relative wavelength shifts in the spatially resolved active-region core spectra. The iron ions are the hottest ions ever used for this type of analysis. All of these lines reveal statistically significant variations in their measured relative wavelength shifts across the active-region core, including mixtures of blueshifts and redshifts. The absence of trends relating velocity with temperature or position indicates a dynamic, turbulent corona: plasma elements on spatial scales comparable to the SERTS spatial resolution move independently of one another.

2. For each of the six lines above we calculated weighted-average relative Doppler velocities from the wavelength shifts in the spatially resolved core spectra (relative to the edge spectrum) by weighting the shifts in the individual spatial pixels with their respective measurement uncertainties. We obtain weighted-average relative velocities of 3.3 ± 1.1 km s^{-1} for He II, 5.2 ± 1.6 km s^{-1} for Fe XII, 0.7 ± 1.5 km s^{-1} for Fe XIII, -2.1 ± 1.4 km s^{-1} for Fe XIV, 1.0 ± 1.1 km s^{-1} for Fe XV, and -1.1 ± 0.8 km s^{-1} for Fe XVI.

3. For each of the six lines above we also calculated intensity-weighted relative Doppler velocities from the wavelength shifts in the spatially averaged core spectrum (relative to the edge spectrum). We obtain intensity-weighted velocities of 5.8 ± 0.6 km s^{-1} for He II, 5.7 ± 0.9 km s^{-1} for Fe XII, 0.4 ± 0.7 km s^{-1} for Fe XIII, -2.1 ± 1.0 km s^{-1} for Fe XIV, 0.8 ± 0.8 km s^{-1} for Fe XV, and -1.1 ± 0.5 km s^{-1} for Fe XVI.

4. Several lines in addition to the above six are strong enough in both the edge and average core spectra to provide centroid measurements that are sufficiently reliable for measuring relative wavelength shifts. Combining these with the above six lines, we find statistically significant net redshifts in the spatially averaged active-region core relative to the edge for lines of He II, Fe X, Fe XI, and Fe XII; lines of Fe XIII and Fe XV show no significant shift while lines of Si XI, Fe XIV, and Fe XVI show a small net blueshift. Where multiple lines are available for a given ion, the directions and (except for Fe XI) magnitudes of the relative shifts are mutually consistent.

5. The net relative blueshift observed in the hottest coronal lines in our sample, combined with the net relative redshift observed in the cooler coronal lines, suggests a net upflow of heated material cospatially and cotemporally with a net downflow of cooler material in the active region.

6. Although the Fe XVI line at 335.41 Å is resolved from the Mg VIII line at 335.23 Å in SERTS spectra, blending may become a problem for CDS quiet-Sun spectra where the Mg VIII contribution could be $\gtrsim 7\%$. The Mg VIII contribution is not expected to exceed $\sim 1\%$ in active-region spectra.

REFERENCES

Achour, H., Brekke, P., Kjeldseth-Moe, O., & Maltby, P. 1995, ApJ, 453, 945
Arnaud, M., & Raymond, J. 1992, ApJ, 398, 394
Behring, W. E., Cohen, L., & Feldman, U. 1972, ApJ, 175, 493
Behring, W. E., Cohen, L., Feldman, U., & Doschek, G. A. 1976, ApJ, 203, 521
Bhatia, A. K., & Thomas, R. J. 1998, ApJ, 497, 483
Brekke, P. 1993, ApJ, 408, 735
Brekke, P., Hassler, D. M., & Wilhelm, K. 1997a, Sol. Phys., 175, 349
Brekke, P., Kjeldseth-Moe, O., Brynildsen, N., Maltby, P., Haugan, S. V. H., Harrison, R. A., Thompson, W. T., & Pike, C. D. 1997b, Sol. Phys., 170, 163
Brekke, P., Kjeldseth-Moe, O., & Harrison, R. A. 1997c, Sol. Phys., 175, 511
Brosius, J. W., Davila, J. M., & Thomas, R. J. 1998, ApJS, 119, 255

Brosius, J. W., Davila, J. M., Thomas, R. J., & Monsignori-Fossi, B. C. 1996, ApJS, 106, 143
Dere, K. P. 1982, Sol. Phys., 77, 77
Dere, K. P., Bartoe, J.-D. F., & Brueckner, G. E. 1984, ApJ, 281, 870
Doschek, G. A., Feldman, U., & Bohlin, J. D. 1976, ApJ, 205, L177
Feldman, U., Cohen, L., & Doschek, G. A. 1982, ApJ, 255, 325
Fuhr, J. R., Martin, G. A., & Wiese, W. L. 1988, J. Phys. Chem. Ref. Data, 17, Suppl. 4
Hassler, D. M., Rottman, G. J., & Orrall, F. Q. 1991, ApJ, 372, 710
Kaufman, V., & Edlen, B. 1974, J. Phys. Chem. Ref. Data, 3, 825
Kelly, R. L. 1987, J. Phys. Chem. Ref. Data, 16, Suppl. 1 (Finding List)
Kelly, R. L., & Palumbo, L. J. 1973, NRL Rept. 7599, (Washington, DC: Naval Research Laboratory)
Thomas, R. J., & Neupert, W. M. 1994, ApJS, 91, 461